Behavior of Electron-Spin Echoes and Photon Echoes in High Fields*

D. Grischkowsky† and S. R. Hartmann‡

Columbia Radiation Laboratory, Department of Physics, Columbia University, New York, New York 10027

The amplitude of the electron-spin or photon echo from an ensemble of isolated atoms (echo atoms) interacting with magnetic-nuclear neighbors is calculated as a function of the magnitude and the orientation of an applied magnetic field $\vec{H}$ and the separation between the two excitation pulses, in the limit that the magnitude of $\vec{H}$ is large compared to the effective local fields at the echo-atom sites due to the nuclear neighbors. The general problem is reduced to the equivalent problem of two-level echo atoms interacting with nuclear neighbors. The latter problem is readily solved and applied to both spin and photon echoes. Experimentally observed spin-echo behavior in ruby is compared to calculated spin-echo behavior using no adjustable parameters, and is found to be in good agreement even when the magnetic field is tilted away from the optic axis thereby causing the echoes to disappear. Calculated photon-echo behavior, in which it is assumed that the interaction constants in the excited state are simply related to those in the ground state, shows the same general features as those that have been observed in experiment. Several results are presented to show the wide range of photon-echo behavior for different values of the interaction constants. A simple theory is presented which explains most observed echo behavior in a straightforward way.

I. INTRODUCTION

Several experiments have been reported in which electron-spin echoes in ionic solids have been studied as a function of excitation pulse separation.[1-4] These experiments were characterized by a modulated echo envelope; the modulation was caused by the interaction between the isolated electron spins and the nearby nuclear magnetic neighbors. Using the density-matrix formalism,[5,6] Rowan, Hahn, and Mims gave the first rigorous theoretical treatment of the echo envelope modulation, where they considered the electron spins to be magnetically coupled to the nuclear neighbors by the isotropic hyperfine coupling and the direct dipole-dipole and pseudodipole anisotropic hyperfine interactions.[3] Their calculation is valid for arbitrary spins for the paramagnetic ion (electron spin) and the nuclear neighbors. Applying the theory to Ce^{3+} in $CaWO_4$ and characterizing the interaction between the electron spin and the nuclear neighbors by only two adjustable parameters, they were able to predict and observe the amplitude, width, and position of the initial dip in the echo envelope as a function of the angle Θ_0 between the magnetic field and the crystal C axis. Zhidomirov and Salikov have theoretically studied the spin-echo envelope for the case of free radicals where the hyperfine structure is resolved.[7]

Recent observations of spin echoes in ruby also showed a modulated echo envelope (Fig. 1), where a straightforward density-matrix calculation similar to that of Rowan, Hahn, and Mims (except for the inclusion of a nuclear electric quadrupole term

which is treated by perturbation theory) led to the good agreement of theory and experiment.[4] However, to study an arbitrary transition between the energy levels of the Cr^{3+} ion with the magnetic field applied in any direction, a more general Hamiltonian had to be considered in the echo calculation, and the theoretical treatment was reformulated to handle this more complicated case in a simple manner. Using the theory developed in this paper, it is possible to treat the Cr^{3+} ion
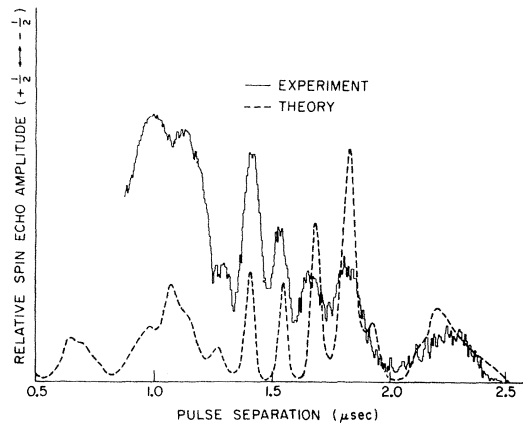

FIG. 1. Comparison of theory and experiment for the amplitude of the spin echoes in ruby versus the separation between the two excitation pulses; there were no adjustable parameters in the theory. The magnetic field of 3.3 kG was applied along the optic axis, and the two excitation pulses had equal widths of approximately 60 nsec (Ref. 4).

as a two-level system, and it is relatively easy to include crystalline field effects, electric quadrupole interactions, and more general energy-level structures in the calculation of the echo behavior. This generalized theory allows the echo envelope for the spin echoes in ruby to be calculated when the mixing of states of the Cr^{3+} ion caused by the crystal-field splitting becomes important ($\Theta \neq 0$, Figs. 4-6) and when the electric quadrupole term is no longer small compared to the other terms in the Hamiltonian for the nuclear neighbor (Fig. 4). No adjustable parameters are incorporated into the ruby spin-echo problem, since the ENDOR work of Laurance, McIrvine, and Lambe[8] provides all the relevant interaction parameters. The theory is also readily applied to the calculation of the photon-echo behavior in ruby.[9-12] The application is presently limited because of our lack of knowledge of the interaction Hamiltonian when the Cr^{3+} ions in Al_2O_3 are in the $\bar{E}(^2E)$ excited state; however, reasonable agreement with experiment is obtained when one assumes comparable interactions in the ground and excited states.

In order to provide insight into the echo-modulation process, a simple model is developed. The essence of this model is that the precessing, but otherwise randomly oriented, nuclear neighbors of the isolated echo atoms provide at the echo-atom sites a quasiperiodic oscillating environment which modulates the energy separation between the two energy levels (echo states) in which the echo is forming and thereby leads to a modulation of the echo envelope.[4]

II. GENERAL THEORY

A quantum-mechanical calculation of the echo behavior, caused by the interaction between the echo atoms and the magnetic nuclear neighbors, is readily performed when static magnetic fields are applied which are large compared to the local magnetic fields at the atomic sites due to the neighbors and when nuclear spin-spin interactions are neglected. The calculation is greatly facilitated by describing the echo atom within the framework of the two levels (echo states) connected by the resonant radiation used to excite the echoes, while taking into account the interaction between the echo atom and the neighboring magnetic nuclei.

The Hamiltonian for a single echo atom in the host crystal, the nuclear neighbors, and the interaction between the echo atom and the neighbors is written

$$\mathcal{H} = \mathcal{H}^0 + \mathcal{H}_R^0 + H^n + \mathcal{H}^I \quad , \tag{2.1}$$

where $\mathcal{H}^0$ describes the interaction between the echo atom and the static environment, and H^n is

the corresponding term for the neighboring nuclei. $\mathcal{H}_R^0$ gives the time-dependent interaction between the atom and the oscillating radiation field. $\mathcal{H}^I$ is the term responsible for the modulation of the echo envelope and describes the interaction between the echo atom and the nuclear neighbors.

The energy separation between the two echo states 1 and 2 of the echo atom is $\hbar\omega_0$, where level 1 has the higher energy. Because we apply intense resonant radiation of angular frequency ω_0, only states 1 and 2 are strongly coupled together, and the influence of the other energy states of the echo atom is considered to be negligible. In many cases, for both electron spin and photon echoes, the interaction between the echo atom and the nuclear neighbors can cause transitions from echo states 1 and 2 to other states of the echo atom and thereby invalidate the two-level approximation. However, the effectiveness of this interaction in causing transitions is strongly field dependent, and if the applied field $\vec{H}$ is large enough compared to the local field at the echo atom site, these transitions do not occur,[11] and the two-level approximation is valid. The following calculations assume approximation is correct. Consequently, the echo calculation can be made within the framework of the two echo states by replacing any operator G by the reduced operator:

$$G = \tfrac{1}{2}\{(G_{11} + G_{22})\sigma_0 + (G_{11} - G_{22})\sigma_3$$
$$+ (G_{12} + G_{21})\sigma_1 + i(G_{12} - G_{21})\sigma_2\} \tag{2.2}$$

for $\quad G_{\alpha\beta} = \langle\alpha | G | \beta\rangle \quad$.

$|1\rangle$ and $|2\rangle$ are the eigenfunctions of $\mathcal{H}^0$ for the echo states 1 and 2, and the σ's are the Pauli matrices. By redefining zero energy for the system of an echo atom and the nuclear neighbors, we obtain the reduced Hamiltonian

$$\mathcal{H} = \tfrac{1}{2}\{(2H^n + H_{11}^I + H_{22}^I)\sigma_0 + (\hbar\omega_0 + H_{11}^I - H_{22}^I)\sigma_3$$
$$+ (H_{R_{12}}^0 + H_{R_{21}}^0)\sigma_1 + i(H_{R_{12}}^0 - H_{R_{21}}^0)\sigma_2\} \quad . \tag{2.3}$$

The terms H_{12}^I and H_{21}^I are set equal to zero, since we consider only the situation where the frequency ω_0, corresponding to the energy separation between the echo states, is very high compared to the precession frequencies of the neighboring nuclei, and the effects of these terms are averaged out.[13] $H_{R_{11}}^0$ and $H_{R_{22}}^0$ are neglected because they do not couple the two echo states.

The echo amplitude is proportional to the ensemble average of the time-dependent part of the expectation value of the dipole moment between the states 1 and 2 after the system has been excited by the two resonant pulses. Let $\vec{P}$ designate the vector operator for the dipole moment of the echo atom and ρ designate the density matrix for the

system; the ensemble average of the expectation value of $\vec{P}$ is then given by

$$\langle \vec{P}(t) \rangle = \mathrm{Tr}\, \vec{P}\, \rho(t) \quad . \tag{2.4}$$

For completeness, we review the essential points of the density-matrix theory which are applicable to our presentation.[5,6] The density matrix ρ satisfies the equation

$$\frac{d\rho}{dt} = \frac{i}{\hbar}[\rho, \mathcal{3C}] \quad . \tag{2.5}$$

When $\mathcal{3C}$ is time independent, Eq. (2.5) has the simple solution

$$\rho(t) = \exp\left(\frac{-i}{\hbar}(t-t_0)\mathcal{3C}\right)$$
$$\times \rho(t_0)\exp\left(\frac{+i}{\hbar}(t-t_0)\mathcal{3C}\right) \quad . \tag{2.6}$$

We apply two short intense resonant pulses of radiation to the system at $t=0$ and at $t=\tau$ and assume that during the application of the pulses H^n and $\mathcal{3C}^I$ can be neglected. Note that when the pulses are turned off, $\mathcal{3C}_R^0$ disappears, and the Hamiltonian $\mathcal{3C}$ is time independent. Thus, the density matrix at time t $(\tau < t)$ is

$$\rho(t) = e^{-i(t-\tau)\mathcal{3C}/\hbar}\, R_2 e^{-i\tau\mathcal{3C}/\hbar}\, R_1 \rho^0 \quad (\mathrm{H.c.}) \quad , \tag{2.7}$$

where R_1 and R_2 give the effect of the excitation pulses, and H.c. is the Hermitian conjugate of the product of operators acting on the initial density matrix ρ^0 from the left. R_1 and R_2 have the form of simple rotation operators, and when the two-pulse sequence is the ideal $90°$–$180°$ series, they are given by

$$R_1 = \exp(-\tfrac{1}{4}i\pi\sigma_2) \quad \text{and} \quad R_2 = \exp(-\tfrac{1}{2}i\pi\sigma_2). \tag{2.8}$$

However, the echo behavior due to the interaction between the echo atoms and the nuclear neighbors is the same for any other two-pulse sequence φ_1 and φ_2 (φ_1 and φ_2 are the angles by which $\vec{P}$ is rotated about the fields of the first and second excitation pulses, respectively), but the strength of the echo is reduced by the factor $\sin\varphi_1\sin^2(\tfrac{1}{2}\varphi_2)$. The Hamiltonian $\mathcal{3C}$ in Eq. (2.7) does not contain $\mathcal{3C}_R^0$, the radiation field interaction term, and we find it convenient to introduce the operator

$$\mathcal{3C}_\pm = \tfrac{1}{2}(2H^n + H_{11}^I + H_{22}^I)\sigma_0 \pm \tfrac{1}{2}(H_{11}^I - H_{22}^I)\sigma_3 \; ; \tag{2.9}$$

the $\pm$ notation will be quite useful. The expression for $\rho(t)$ now becomes

$$\rho(t) = \{\exp[-\tfrac{1}{2}i(t-2\tau)\omega_0\sigma_3]\}\{\exp[-i(t-\tau)\mathcal{3C}_+/\hbar]\}R_2\{\exp[-i\tau\mathcal{3C}_+/\hbar]\}R_1\rho^0 \quad (\mathrm{H.c.}) \quad . \tag{2.10}$$

The operator ρ^0 for the initial density matrix of the system before any pulses are applied can be written

$$\rho^0 = [\tfrac{1}{2}\sigma_0 - \tfrac{1}{2}\sigma_3\tanh(\hbar\omega_0/2kT)]\Pi_j(2I_j+1)^{-1} \quad , \tag{2.11}$$

where the ensemble of echo atoms is assumed to have temperature T and the nuclear neighbors are treated by the high-temperature approximation. The index j refers to the jth neighbor, and I_j is the nuclear spin quantum number. Because the echo amplitude is proportional to the time-dependent part of $\langle \vec{P}(t)\rangle$, only the time-dependent part of the density matrix is important for the echo calculation, and the first term of the initial density matrix, which allows all of the time-development operators to collapse, can be neglected. Recalling that $\exp(-i\varphi\sigma_2)$ describes a rotation of 2φ rad and using the identity

$$\sigma_1 = -i\exp(+\tfrac{1}{2}i\pi\sigma_1) \quad , \tag{2.12}$$

we can change Eq. (2.10) to

$$\rho(t) = \tfrac{1}{2}\tanh\tfrac{1}{2}(\hbar\omega_0/kT)\Pi_j(2I_j+1)^{-1}\sigma_1\exp[i(t-2\tau)\omega_0\sigma_3]\exp[-i(t-\tau)\mathcal{3C}_-/\hbar]$$
$$\times\exp[-i\tau\mathcal{3C}_+/\hbar]\exp[+i\tau\mathcal{3C}_-/\hbar]\exp[+i(t-\tau)\mathcal{3C}_+/\hbar] \quad . \tag{2.13}$$

We now define new operators H_1 and H_2, so that $\mathcal{3C}_\pm$ can be written more symmetrically as

$$\mathcal{3C}_\pm = \tfrac{1}{2}(H_1+H_2)\sigma_0 \pm \tfrac{1}{2}(H_1-H_2)\sigma_3 \quad . \tag{2.14}$$

Because we neglect interactions among the nuclear neighbors, the Hermitian operators H_1 and H_2 are decomposable into two series of Hermitian operators; each operator in a series acts on a single nuclear neighbor.

$$H_1 = H^n + H_{11}^I = \sum_j h_1^j \quad \text{and} \quad H_2 = H^n + H_{22}^I = \sum_j h_2^j \quad . \tag{2.15}$$

The commutation relations $\quad [h_1^i, h_1^j] = [h_1^i, h_2^j] = [h_2^i, h_2^j] = 0 \tag{2.16}$

are satisfied by these operators for $i \neq j$. The indices i and j refer to the ith and jth nuclear neighbors,

respectively. Using Eq. (2.14), we can expand Eq. (2.13) as

$$\rho(t) = \tfrac{1}{4} \tanh(\hbar\omega_0/2kT)\{((C+C^\dagger)\cos[(t-2\tau)\omega_0] + i(C-C^\dagger)\sin[(t-2\tau)\omega_0])\sigma_1$$

$$+ (-i(C-C^\dagger)\cos[(t-2\tau)\omega_0] + (C+C^\dagger)\sin[(t-2\tau)\omega_0])\sigma_2\} , \tag{2.17}$$

with $C = \Pi_j (2I_j+1)^{-1} \exp[-i(t-\tau)H_2/\hbar]\exp[-i\tau H_1/\hbar]\exp[+i\tau H_2/\hbar]\exp[+i(t-\tau)H_1/\hbar]$.   (2.18)

Referring to Eq. (2.15), we note that $C = \Pi_j C_j$,   (2.19)

with $C_j = (2I_j+1)^{-1}\exp[-i(t-\tau)h_2^j/\hbar]\exp[-i\tau h_1^j/\hbar]\exp[i\tau h_2^j/\hbar]\exp[i(t-\tau)h_1^j/\hbar]$.   (2.20)

$\langle\vec{P}(t)\rangle$ given by Eq. (2.4) can be written

$$\langle\vec{P}(t)\rangle = \tfrac{1}{4}\tanh(\hbar\omega_0/2kT)\Pi_j \operatorname{Tr}\{[\vec{P}_{12}+\vec{P}_{21}][(C_j+C_j^\dagger)\cos(t-2\tau)\omega_0 + i(C_j-C_j^\dagger)\sin(t-2\tau)\omega_0]$$

$$+[\vec{P}_{12}-\vec{P}_{21}][(C_j-C_j^\dagger)\cos(t-2\tau)\omega_0 + i(C_j+C_j^\dagger)\sin(t-2\tau)\omega_0]\} , \tag{2.21}$$

which reduces to the relatively simple equation

$$\langle\vec{P}(t)\rangle = \tanh(\hbar\omega_0/2kT)$$
$$\times \operatorname{Re}\exp[i(t-2\tau)\omega_0]\vec{P}_{12}\Pi_j\operatorname{Tr}C_j . \tag{2.22}$$

Equation (2.22)[13a] is the central result of this section. The magnitude of the oscillating dipole moment at $t=2\tau$ (and hence the echo amplitude) is expressed quite simply by Eq. (2.22) in terms of $\vec{P}_{12}$, the matrix element of the dipole moment between the two echo states, and $\Pi_j\operatorname{Tr}C_j$, the product of the traces of C_j for each nuclear neighbor. In simple cases, $\operatorname{Tr}C_j$ can be evaluated exactly, and for the more difficult cases $\operatorname{Tr}C_j$ can be evaluated numerically. The echo behavior due to the interaction between the echo atom and the nuclear neighbors is completely determined by $\Pi_j\operatorname{Tr}C_j$, and in the following sections $\Pi_j\operatorname{Tr}C_j$ is evaluated for the two particular cases of electron-spin and photon echoes in ruby.

The echo occurs at $t\approx 2\tau$, and for evaluation of the echo signal the slowly varying term C_j is set equal to

$$C_j = (2I_j+1)^{-1}\exp[-i\tau h_2^j/\hbar]\exp[-i\tau h_1^j/\hbar]$$
$$\times \exp[+i\tau h_2^j/\hbar]\exp[+i\tau h_1^j/\hbar] . \tag{2.23}$$

Because C_j is a product of functions of the operators h_1^j and h_2^j, it is necessary that we be able to diagonalize these operators. Accordingly, we define $^jU_1$ and $^jU_2$ so that

$$^jU_1 h_1^j \, ^jU_1^\dagger = h_{1D}^j \quad \text{and} \quad ^jU_2 h_2^j \, ^jU_2^\dagger = h_{2D}^j , \tag{2.24}$$

where h_{1D}^j and h_{2D}^j are diagonal matrices. All of the results are being derived for the jth neighbor; however, to keep the number of indices to a minimum, the j subscripts and superscripts will be dropped. The trace of C_j can be put in the form

$$\operatorname{Tr}C_j = (2I_j+1)^{-1}\operatorname{Tr}U_2^\dagger U_2 \exp[-i\tau h_2/\hbar]$$

$$\times U_2^\dagger U_2 U_1^\dagger U_1 \exp[-i\tau h_1/\hbar]U_1^\dagger U_1 U_2^\dagger U_2$$

$$\times \exp[+i\tau h_2/\hbar]U_2^\dagger U_2 U_1^\dagger U_1 \exp[+i\tau h_1/\hbar]U_1^\dagger U_1 , \tag{2.25}$$

which is equivalent to

$$\operatorname{Tr}C_j = (2I_j+1)^{-1}\operatorname{Tr}\exp[-i\tau h_{2D}/\hbar]W$$

$$\times\exp[-i\tau h_{1D}/\hbar]W^\dagger\exp[+i\tau h_{2D}/\hbar]W$$

$$\times\exp[i\tau h_{1D}/\hbar]W^\dagger , \tag{2.26}$$

with $W = U_2 U_1^\dagger$. W is a time-independent unitary matrix; all of the time dependence is carried by the diagonal matrices. Equation (2.26) can be written in a form more suitable for direct evaluation as

$$\operatorname{Tr}C_j = (2I_j+1)^{-1}\!\left(\sum_{\alpha,\gamma,\lambda,\epsilon}^{2I+1}\{\cos[\tau(h_{2D_\alpha}-h_{2D_\lambda})/\hbar]\right.$$

$$\times\cos[\tau(h_{1D_\gamma}-h_{1D_\epsilon})/\hbar] - \sin[\tau(h_{2D_\alpha}-h_{2D_\lambda})/\hbar]$$

$$\left.\times\sin[\gamma(h_{1D_\gamma}-h_{1D_\epsilon})/\hbar]\}W_{\alpha\gamma}W_{\alpha\epsilon}^* W_{\lambda\gamma}W_{\lambda\epsilon}\right)_j , \tag{2.27}$$

with $(h_{1D})_{\alpha\alpha} = h_{1D_\alpha}$ and $(h_{2D})_{\beta\beta} = h_{2D_\beta}$.

h_{1D_α} or h_{2D_β} are the energy eigenvalues of the jth nuclear neighbor with the echo atom in echo state 1 or 2, respectively. $W_{\alpha\epsilon}^*$ is the complex conjugate of the matrix element $W_{\alpha\epsilon}$. The summation indices α, γ, λ, and ϵ are independent and range from 1 to $2I+1$, where I is the nuclear spin quantum number. The j subscript on the right indicates that all the quantities in the brackets must be evaluated for the jth nuclear neighbor. The evaluation of $\operatorname{Tr}C_j$ yields the echo amplitude through Eq. (2.22).

It is interesting to note that $\operatorname{Tr}C_j$ is expressible as a summation of products of pairs of sines and cosines with each pair having one term oscillating at a precession frequency associated with the echo atom being in the ground state (echo state 2) and

the other term oscillating at a precession frequency associated with the echo atom being in the excited state (echo state 1).

III. SPIN ECHOES IN RUBY

A. Theory

Using the general theory of Sec. II as our basic theoretical framework, we will calculate the spin-echo behavior in ruby due to the interactions between the paramagnetic Cr^{3+} ions and the Al nuclear neighbors. The electron-spin echoes are associated with the various allowed transitions between the different spin states (shown in Fig. 2) of the Cr^{3+} ion. The Hamiltonian describing a single Cr^{3+} impurity ion in Al_2O_3 (ruby) and the Al neighbors is considered to have the form[8]

$$\mathcal{H} = g\mu_B \vec{H} \cdot \vec{S} + D[(S_z)^2 - \tfrac{1}{3}S(S+1)]$$
$$+ \sum_j \{ -\hbar\gamma \vec{H} \cdot \vec{I}_j + Q^j[(I_{zj})^2 - \tfrac{1}{3}I(I+1)]\}$$
$$+ \vec{S} \cdot \sum_j \{ A_j \vec{I}_j + B_j[3\vec{r}_j(\vec{I}_j \cdot \vec{r}_j)/r_j^5 - \vec{I}_j/r_j^3]\} \ . \ (3.1)$$

For Eq. (3.1), the z axis is parallel to the axis of trigonal symmetry (the optic axis) for the crystal, and the Cr^{3+} ion is located at the origin of coordinates. The g value for Cr^{3+} is considered to be isotropic with $g = 1.984$; μ_B is the Bohr magneton. The symbol D is the measure of the crystal-field splitting, and $2D/\hbar = -11.493$ GHz. The summation is taken over the 13 nearest Al neighbors. $\vec{S}$ and $\vec{I}_j$ are the spin operators for the Cr^{3+} ion and the jth Al nucleus, respectively, where the Cr^{3+} ion has spin $\tfrac{3}{2}$ and the Al neighbors have nuclear spin $\tfrac{5}{2}$. $\vec{H}$ is the applied magnetic field; $\gamma/2\pi$ for the Al nucleus is 11.094 MHz for a field of 10 kG. In Table I, we give the values of A_j, B_j, Q^j, and $\vec{r}_j$ used in our computer calculations. The constants A_j, B_j, and Q^j for the 13 nearest neighbors have been determined from earlier ENDOR work (Table
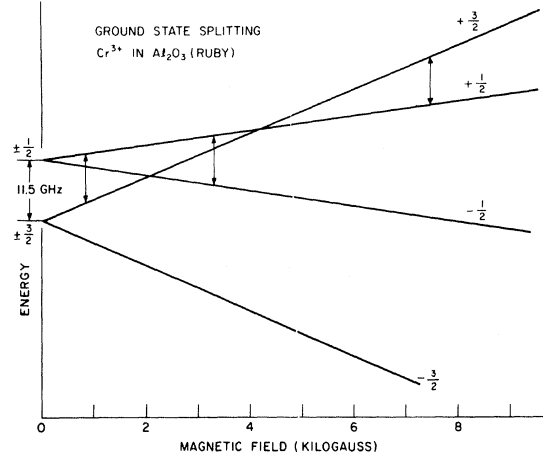

FIG. 2. Splitting of the $^4A_2$ ground state of the Cr^{3+} ion versus the strength of the magnetic field applied along the optic axis. The three arrows indicate the allowed transitions at 9.25 GHz.

4 of Laurance et al.[8]) by the relations

$$A_j = h[(A+B_z)_{expt} - (B_t \ expt/B_t \ point)B_z \ point] \times 10^6,$$
$$B_j = (B_t \ expt/B_t \ point)\mu_B g \hbar \gamma \ , \qquad (3.2)$$
$$Q^j = hQ' \times 10^6 \ ,$$

where the subscript expt refers to their experimental values given in MHz and the subscript point refers to their calculated result for a point dipole. The position vectors $\vec{r}_j$ with components (x_j, y_j, z_j) of the nuclear neighbors with the Cr^{3+} ion at the origin of coordinates have been obtained from Table 1 of Ref. 8. Laurance et al. designate the four sets of equivalent nuclear neighbors as sets I, J, K, and L and the nearest neighbor by G. In our notation set I corresponds to neighbors 1–3; set J corresponds to neighbors 4–6; set K corresponds to neighbors 7–9; set L corresponds to

TABLE I. Parameters A_j, B_j, Q^j, and $\vec{r}_j$ for the 13 nearest Al neighbors of the Cr^{3+} ion in ruby.

Nuclear neighbor j	A_j $(10^{-20}$ erg$)$	B_j $(10^{-43}$ erg cm$^3)$	Q^j $(10^{-20}$ erg$)$	x_j $(10^{-8}$ cm$)$	y_j $(10^{-8}$ cm$)$	z_j $(10^{-8}$ cm$)$
1	2.04	1.08	0.093	+1.380	+2.380	−0.560
2	2.04	1.08	0.093	+1.380	−2.380	−0.560
3	2.04	1.08	0.093	−2.751	0.0	−0.560
4	1.56	1.72	0.113	+2.751	0.0	−2.170
5	1.56	1.72	0.113	−1.380	+2.380	−2.170
6	1.56	1.72	0.113	−1.380	−2.380	−2.170
7	1.46	1.36	0.096	+2.751	0.0	+1.600
8	1.46	1.36	0.096	−1.380	+2.380	+1.600
9	1.46	1.36	0.096	−1.380	−2.380	+1.600
10	0.86	1.70	0.116	+1.380	+2.380	+2.170
11	0.86	1.70	0.116	+1.380	−2.380	+2.170
12	0.86	1.70	0.116	−2.751	0.0	+2.170
13	0.45	1.35	0.175	0.0	0.0	−2.730

neighbors 10–12, and G corresponds to neighbor 13.

We diagonalize the spin Hamiltonian[14] for the Cr^{3+} ion and obtain the four eigenstates. However, we are only concerned with the eigenfunctions designated as $|1\rangle$ and $|2\rangle$, which are involved in the spin-echo formation. Note that when the angle Θ between the optic axis and $\vec{H}$ is not zero, the states $|1\rangle$ and $|2\rangle$ are not eigenfunctions of $S_{\vec{z}}$, and the vectors $\vec{S}_{11}$ and $\vec{S}_{22}$ are not parallel to $\vec{H}$. Equation (2.4) gives the spin-echo amplitude with $\vec{P}$ the dipole moment operator given by

$$\vec{P} = -g\mu_B\vec{S} \quad . \tag{3.3}$$

The evaluation of $\mathrm{Tr}C_j$ for spin echoes is accomplished by writing $h_{1,2}^j$ of Eq. (2.15) as

$$h_{1,2}^j = \hbar\gamma\left[\vec{H} - \frac{A_j\vec{S}_{11,22}}{\hbar\gamma} - \frac{B_j}{\hbar\gamma_i}\left(\frac{3\vec{r}_j(\vec{S}_{11,22}\cdot\vec{r}_j)}{r_j^5}\right.\right.$$
$$\left.\left. - \frac{\vec{S}_{11,22}}{r_j^3}\right)\right]\cdot\vec{I}_j + Q_j\{I_{zj}^2 - \tfrac{1}{3}[I(I+1)]\} \quad . \tag{3.4}$$

Equation (3.4) and the following equations are actually two separate equations, one for h_1^j and the other for h_2^j, according to whether one uses only the 1 or 2 indices, respectively. Equation (3.4) can be recast into a form which uses the concept of the effective magnetic fields[8] $\vec{H}_{ej}^{1,2}$ at the jth Al neighbor.

$$h_{1,2} = -\hbar\gamma|\vec{H}_e^{1,2}|(I_x\sin\eta_{1,2}\cos\chi_{1,2} + I_y\sin\eta_{1,2}\sin\chi_{1,2}$$
$$+ I_z\cos\eta_{1,2}) + Q[I_z^2 - \tfrac{1}{3}I(I+1)]; \tag{3.5}$$

the j indices are neglected for clarity. We write the operators $U_{1,2}$ of Eq. (2.24), which diagonalize $h_{1,2}$ as the products

$$U_{1,2} = V_{1,2}T_{1,2} \quad , \tag{3.6}$$

where $T_{1,2}$ are simple rotation operators such that

$$T_{1,2}h_{1,2}T_{1,2}^\dagger = -\hbar\gamma|\vec{H}_e^{1,2}|(I_x\sin\eta_{1,2}$$
$$+ I_z\cos\eta_{1,2}) + Q[I_z^2 - \tfrac{1}{3}I(I+1)] \quad . \tag{3.7}$$

Equation (3.7) defines two real symmetric, 6×6 matrices which are easily diagonalized numerically to yield $h_{1D,2D}$ and $V_{1,2}$. The $\mathrm{Tr}C_j$ is then obtained from Eq. (2.27).

B. Experiment

The spin-echo spectrometer is shown schematically in Fig. 3. The sample is contained in the low-Q balanced bimodal cavity, which is immersed in liquid helium, and the two microwave excitation pulses are generated by the magnetron mechanically tuned to the cavity frequency. During the excitation pulses, the receiver is protected by the three units in front of the mixer; the limiter, the isolator, and the Hewlett-Packard PIN modulator. After the
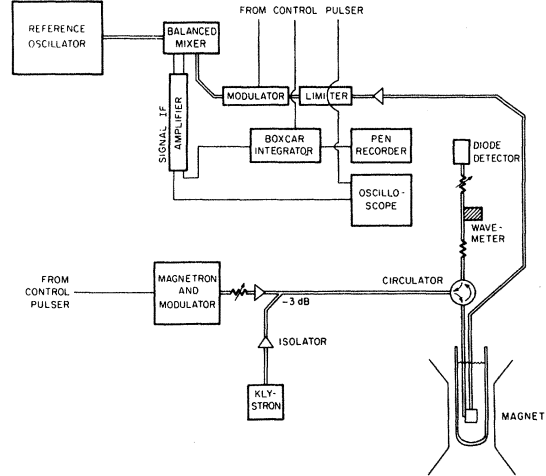

FIG. 3. Spin-echo spectrometer.

two pulses, the attenuation due to the PIN modulator is turned off, thereby effectively connecting the receiver to the output waveguide of the bimodal cavity. If an echo is formed, the oscillating magnetization of the sample spontaneously rephases and then dephases, and a microwave echo pulse at the cavity frequency is radiated by the sample. The echo pulse is mixed with the continuous reference signal with a frequency 30 MHz above or below the cavity frequency, and an i.f. output pulse is emitted by the balanced mixer at the difference frequency. This 30-MHz pulse is amplified by the signal i.f. amplifier and observed with the oscilloscope, or the amplified pulse is detected and put into the boxcar integrator, which is pulsed on during the echo pulse. The dc output of the boxcar is proportional to the amplitude of the detected echo pulse. The gating pulse to the boxcar is 0.5 μsec wide and the i.f. amplifier has a bandpass of 2 MHz. The data taking is completely automated; the spacing between the two excitation pulses is slowly changed by a clock motor, and the magnitudes of the resulting echo pulses are recorded by a chart recorder connected to the boxcar output. The resulting record gives the echo amplitude versus the separation between the two excitation pulses.

Several initial attempts to observe electron-spin echoes in ruby at liquid-helium temperatures were unsuccessful. With reference to other related experiments,[8,9] it was inferred that the magnetic field $\vec{H}$ should be applied precisely along the optic axis of the crystal and that the concentration of the Cr^{3+} ion should be reduced. When the concentration of Cr_2O_3 was reduced from 0.05 to 0.005% by weight and $\vec{H}$ was applied parallel to the optic axis of the crystal, echoes were observed. $\vec{H}$ was aligned parallel to the optic axis by monitoring the
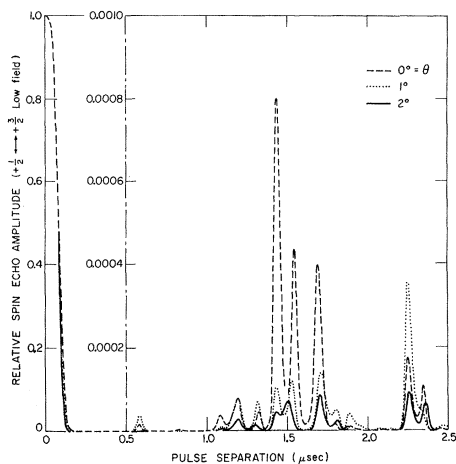
FIG. 4. Theoretical dependence for the $(+\frac{1}{2} \longleftrightarrow +\frac{3}{2}$ low-field) transition at 9.25 GHz shown in Fig. 2, of the amplitude of the spin echoes in ruby on the separation between the two excitation pulses as the angle θ between the optic axis and the magnetic field is increased. Note the scale changes at 0.5 μsec.

resonance signal associated with the "forbidden" $(+\frac{3}{2} \longleftrightarrow -\frac{1}{2})$ transition and by adjusting the orientation of $\vec{H}$ for minimum signal. Because of the long spin-lattice relaxation time of the Cr^{3+} ion in ruby at liquid-helium temperatures, the repetition rate for echo production had to be of the order of one pulse series per sec.

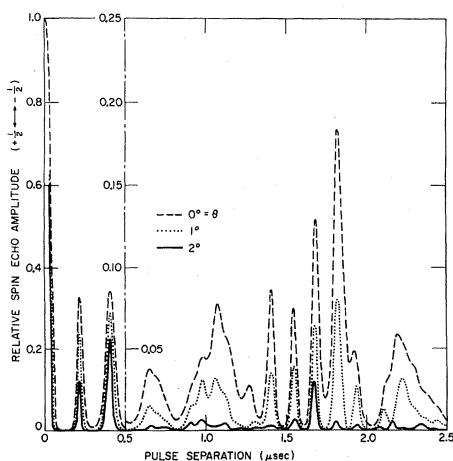## C. Results

The theoretical dependence of the spin-echo

FIG. 5. Theoretical dependence, for the $(+\frac{1}{2} \longleftrightarrow -\frac{1}{2})$ transition at 9.25 GHz shown in Fig. 2, of the amplitude of the spin-echoes in ruby on the separation between the two excitation pulses as the angle θ between the optic axis and the magnetic field is increased. Note the scale changes at 0.5 μsec.
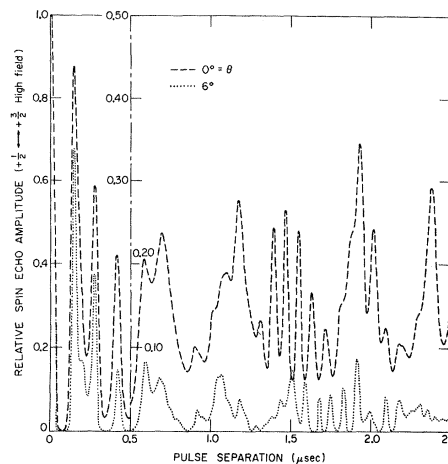
FIG. 6. Theoretical dependence, for the $(+\frac{1}{2} \longleftrightarrow +\frac{3}{2}$ high-field) transition at 9.25 GHz shown in Fig. 2, of the amplitude of the spin echoes in ruby on the separation between the two excitation pulses as the angle θ between the optic axis and the magnetic field is increased. Note the scale changes at 0.5 μsec.

amplitude on the separation τ between the two excitation pulses and on the angle Θ between the applied magnetic field $\vec{H}$ and the optic axis of the ruby crystal is presented in Figs. 4–6 for the three allowed transitions at 9.25 GHz, which are indicated by the arrows in Fig. 2. Figures 4–6 show the same general behavior: The amplitude of the echo signal is modulated as τ is changed, and the echo signal is reduced as Θ is increased. Also, the average echo signal increases as $\vec{H}$ is raised from the low-field transition to the high-field transition. Figure 7 shows the separate contributions $(\text{Re Tr}C_j)$ from each nuclear-neighbor type to the modulation pattern. With $\Theta = 0$ there are three neighbors of each type, and the modulation is given by the product of the curves for each type raised to the third power. The result $(\text{Re} \Pi_j \text{ Tr}C_j)$ is the bottom curve of Fig. 7, which is compared with experiment in Fig. 1. The theoretical curves have been normalized to unity for zero pulse separation and are proportional to the real part of $\Pi_j \text{Tr}C_j$ [see Eqs. (2.22) and (2.27)], as the imaginary part is negligible for small Θ. For the three transitions, the magnitude of $\vec{H}$ was adjusted to maintain the energy separation of 9.25 GHz between the two states involved in the echo formation as Θ was changed. The echo amplitude shows a minor dependence on the angular orientation of the plane containing $\vec{H}$ and the optic axis. However, with certain exceptions the major features of the theoretical curves are essentially unchanged as $\vec{H}$ is rotated about the optic axis with Θ kept constant. No adjustable parameters were involved in the
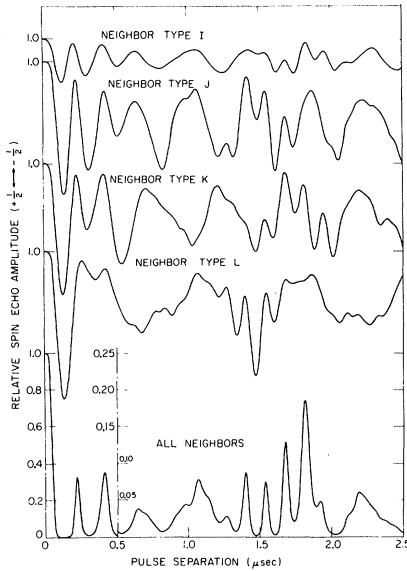
Fig. 7

FIG. 7. Decomposition of the theoretical spin-echo envelope modulation for the $(+\frac{1}{2} \longleftrightarrow -\frac{1}{2})$ transition at 9.25 GHz with $\theta = 0$, which shows the modulation that would be observed if the Cr^{3+} ion interacted with a single Al nuclear neighbor of type I, J, K, or L, (Ref. 8) respectively. Since there are three neighbors of each type, the theoretical modulation pattern (the bottom curve) is the product of the curves for each neighbor type raised to the third power.

computations.

Spin echoes at 9.25 GHz were observed in dilute ruby at liquid-helium temperatures with the magnetic field applied essentially parallel to the optic axis of the crystal.[4] The echoes could only be seen for the $(+\frac{1}{2} \longleftrightarrow -\frac{1}{2})$ transition at 3.3 kG; no echoes could be seen for the $(+\frac{1}{2} \longleftrightarrow +\frac{3}{2}$ low-field) transition at 0.8 kG, and we were unable to look for the echoes of the $(+\frac{1}{2} \longleftrightarrow +\frac{3}{2}$ high-field) transition as our magnet could not produce the required field. Our negative results for the echoes of the $(+\frac{1}{2} \longleftrightarrow +\frac{3}{2}$ low-field) transition show that the low-field echo signals are less than $\frac{1}{400}$ of the signals for the echoes of the $(+\frac{1}{2} \longleftrightarrow -\frac{1}{2})$ transition with pulse separations from 1 to 2.5 μsec. Figures 4 and 5 show that the theoretical echo signals for the $(+\frac{1}{2} \longleftrightarrow +\frac{3}{2}$ low field) transition are of the order of $\frac{1}{200}$ of the signals for the echoes of the $(+\frac{1}{2} \longleftrightarrow -\frac{1}{2})$ transition. However, the theory includes no relaxation processes, and if the neglected relaxation processes are more important for the $(+\frac{1}{2} \longleftrightarrow +\frac{3}{2}$ low-field) transition than for the $(+\frac{1}{2} \longleftrightarrow -\frac{1}{2})$ transition, the ratio of the echo signals from these two transitions would be smaller than theory predicts.

The amplitude of the echo signal for the $(+\frac{1}{2} \longleftrightarrow -\frac{1}{2})$ transition was strongly modulated[4] as τ was

varied, and the modulation was quite dependent on the width of the excitation pulses. As shown in Fig. 8, the modulation of the echo envelope had much finer detail as the two pulses were made narrower. Increasing the width of the two excitation pulses seemed to merely smear out the details of the short-pulse modulation pattern in a relatively smooth manner. No basic changes in the pattern occurred other than loss of detail as the pulse widths were increased. To rigorously satisfy the short-pulse condition, the width of the excitation pulses must be small compared to the shortest precession period of the nuclear neighbors. However, for excitation pulses of 100 nsec which were approximately one-half the fastest nuclear period the pattern became relatively insensitive to further reductions in pulse width. Thus, the rigorous short-pulse condition seems too stringent. In Fig. 1, experiment and theory agree quite well for the location of the maxima and minima in the modulation patterns. The agreement is especially important since there are no adjustable parameters in the theory. Experiment (Fig. 8) and theory roughly agree for pulse separations between 2.5 and 3.5 μsec but not in detail. This breakdown of agreement as the pulse separation is increased is to be expected, because as the pulse separation is increased the separation corresponds to more and more nuclear periods and small differences between the correct precession frequencies and those put in the theory lead to major discrepencies. The modulation patterns do not agree for the relative
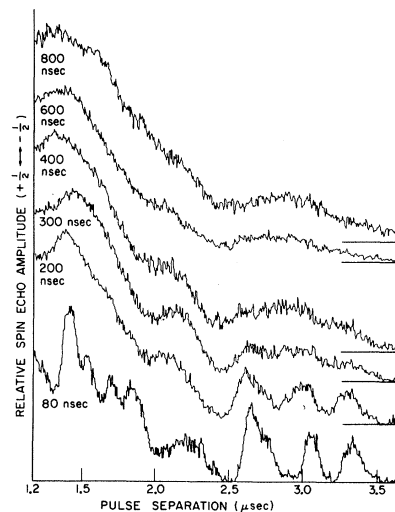

FIG. 8. Measured amplitude of the spin echoes in ruby [for the $(+\frac{1}{2} \longleftrightarrow -\frac{1}{2})$ transition at 9.25 GHz with $\theta = 0$] versus the separation between the two excitation pulses for different durations of the pulses; the two pulses have the same width.

strengths of the echoes. One reason for this dis-
agreement is that the strengths of the relative
maxima for the echo modulation pattern depend on
the B_j parameters, which have an uncertainty of
approximately 10%. Also the theoretical calcula-
tions neglect the $Cr^{3+} \leftrightarrow Cr^{3+}$ interactions and the
$Al \leftrightarrow Al$ interactions. There are no relaxation
mechanisms in the theory.

As shown in Fig. 9, the echo signals rapidly
disappeared as Θ was increased. For the data of
Fig. 9, the magnetic field was readjusted for res-
onance at each different angular setting, because
the position of the line shifts when Θ is changed.
The echoes could no longer be seen when Θ was
greater than $3°$, which corresponded to a reduction
in the echo signal of about 100. A comparison of
the experimental results of Fig. 9 with the theo-
retical predictions of Fig. 5 shows that the ob-
served echoes are not as dependent on Θ as theory
predicts. This reduction in the Θ dependence is
mainly due to the optic axis wandering (of the order
of $1°$) in our crystals which tends to smear out the
sharp Θ behavior.

IV. PHOTON ECHOES IN RUBY

A. Theory

The photon echoes are associated with the vari-
ous allowed transitions between the Zeeman com-
ponents (shown in Fig. 10) of the $\overline{E}(^2E)$ excited
state and the $^4A_2$ ground state of the Cr^{3+} ion. The
photon-echo behavior due to the interaction between

FIG. 10. Splitting of the $\overline{E}$ (^2E) excited state and the
$^4A_2$ ground state of the Cr^{3+} ion versus the strength of
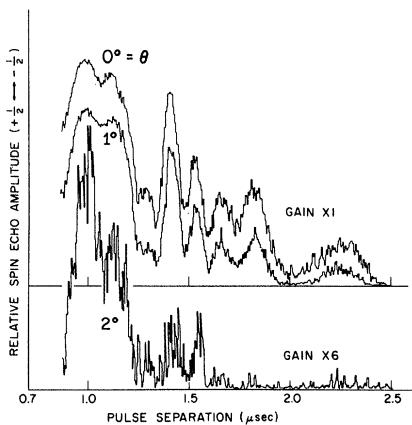the magnetic field applied along the optic axis.

FIG. 9. Measured amplitude of the spin echoes in
ruby versus the separation between the two excitation
pulses as the angle θ between the optic axis and the
magnetic field of approximately 3.3 kG is increased.
The two excitation pulses had equal widths of approxi-
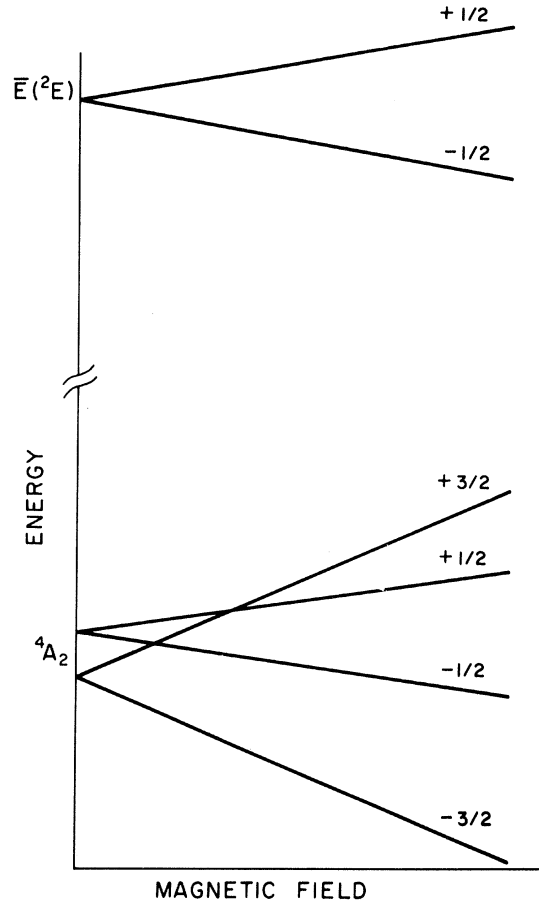mately 60 nsec. Note that for the $\theta = 2°$ curve, the
gain has been increased by 6.

the Cr^{3+} ions and the Al nuclear neighbors will be
obtained for the echoes associated with transitions
between any two Zeeman components designated
as 1 and 2, where 1 is a component of the $\overline{E}(^2E)$
excited state and 2 is a component of the $^4A_2$ ground
state. For simplicity the crystal size is assumed
small compared to λ^3 (the wavelength of the reso-
nant radiation). The calculation is easily extended
to large samples, but the results, except for di-
rectional effects, are the same.[10]

The Hamiltonian $\mathcal{K}$ for the Cr^{3+} ion and the Al
nuclear neighbors has the form of Eq. (2.1), and
for photon echoes $\mathcal{K}^0$ can be split up into the two
terms

$$\mathcal{K}^0 = \mathcal{K}_E^0 + \mathcal{K}_S^0 \quad . \tag{4.1}$$

$\mathcal{K}_E^0$ contains the major terms of the Hamiltonian
for the Cr^{3+} ion and is diagonalized to yield the $^4A_2$
ground state and the first excited state $\overline{E}(^2E)$. The
interaction of the Cr^{3+} ion with $\vec{H}$ is included in $\mathcal{K}_S^0$

which can be treated as a small perturbation. The application of $\vec{H}$ splits the $\bar{E}(^2E)$ level into the two Zeeman components $\psi(^2E, +\frac{1}{2}, -1)$ and $\psi(^2E, -\frac{1}{2}, +1)$, where $\pm\frac{1}{2}$ is the spin quantum number and ± 1 is an orbital quantum number which describes the rotation properties of the wave functions about the optic axis of the crystal.[15,16] The perturbation of the excited state caused by $\mathcal{3C}_S^0$ can be represented by the spin Hamiltonian[17]

$$\mathcal{3C}_S^1 = g_{\parallel}\,\mu_\beta H_z S_z + g_\perp\,\mu_\beta(H_x S_x + H_y S_y) \quad , \tag{4.2}$$

where the z axis is the optic axis of the crystal, the effective spin is $\frac{1}{2}$, and

$$g_{\parallel} = 2.445 \quad \text{and} \quad g_\perp \lesssim 0.06 \quad . \tag{4.3}$$

Because we are only concerned with the situation where the angle Θ is relatively small, Eq. (4.2) can be simplified to

$$\mathcal{3C}_S^1 = g_{\parallel}\,\mu_\beta H_z S_z \quad , \tag{4.4}$$

which is diagonal. The effect of $\mathcal{3C}_S^0$ on the $^4A_2$ ground state is given by the spin Hamiltonian used earlier in the spin-echo calculation.

Since the echo signal is proportional to the radiated power, the intensity of the photon echo is proportional to $\langle\vec{P}(t)\rangle^2$ of Eq. (2.22), where $\vec{P}_{12}$ is the matrix element of the electric-dipole moment operator $\vec{P}$ between the Zeeman components 1 and 2 involved in the echo formation. For evaluation of the $\mathrm{Tr}C_j$ we assume that the terms $h_{1,2}^j$ have the form of Eq. (3.4) for both the excited and ground states of the ion, but that the interaction parameters A_j^* and B_j^* (values unknown) for the excited state are different from those of the ground state, A_j and B_j, which are known. Because each of the Zeeman components of the excited state has a different orbital function, A_j^* and B_j^* are assumed to be different for each component. $\vec{S}_{11}$ is considered to be $\pm\frac{1}{2}\vec{e}_3$ according to whether $\psi(^2E, \pm\frac{1}{2}, \mp 1)$ is designated as state 1. With these considerations, $\mathrm{Tr}C_j$ is given by the result of the spin-echo calculation.

In order to get some familiarity with the predictions of the theory and to keep the problem manageable, the following simplifications are made. As the separation between the two excitation pulses is short compared to the frequencies associated with the electric quadrupole interaction term, this term is neglected by setting $Q^j = 0$. B_j^* is assumed to be given by the dipolar interaction as

$$B_j^* = g_{\parallel}\,\mu_\beta\mu_N g_n \quad . \tag{4.5}$$

$g_n = 1.456$ for Al^{27}, and μ_N is the nuclear magneton. A_j^* is assumed to be proportional to A_j with the same constant of proportionality for all the neighbors, i.e.,

$$A_j^* = A_j(A^*/A) \quad , \tag{4.6}$$

and in the theoretical curves, A^*/A is the only adjustable parameter. Because $Q_j = 0$ in the computations, the $\Pi_j \mathrm{Tr}C_j$ is real; all the theoretical curves of this section are proportional to the square of $\Pi_j\,\mathrm{Tr}C_j$.

B. Results

The results are presented for the theoretical dependence of the intensity of the photon echoes on the angle Θ between the applied magnetic field $\vec{H}$ and the optic axis (Θ dependence), on $\vec{H}$ ($\vec{H}$ dependence), and on the separation τ between the two excitation pulses (τ dependence). We are primarily interested in the theoretical behavior for the $(+\frac{1}{2} \longleftrightarrow +\frac{1}{2})\sigma^-$ and $(-\frac{1}{2} \longleftrightarrow -\frac{1}{2})\sigma^+$ transitions because the $\sigma^\pm$ photon echoes have been studied experimentally.[9-12,18] The experiments used linearly polarized excitation radiation, and the observed signal was due to both σ^+ and σ^- echoes of unknown relative intensity. Thus, a precise comparison with theory is impossible; however, the data are very useful for setting limits on the theoretical parameters. Because the theoretical $\vec{H}$ and Θ dependence of the σ^+ and σ^- echoes are qualitatively similar, only the σ^+ results are presented; both transitions are considered when the τ dependence is discussed. The Θ dependence of theory and experiment are compared in Figs. 11 and 12. For these curves, H_z, the component of $\vec{H}$ along the optic axis, was kept constant, and Θ was varied by increasing the transverse component in order to duplicate the conditions of the experiment.[10] Each curve was independently normalized to unity at $\Theta = 0$. An important feature of these curves is that values of the interaction parameter A^*/A of the order of unity give reason-
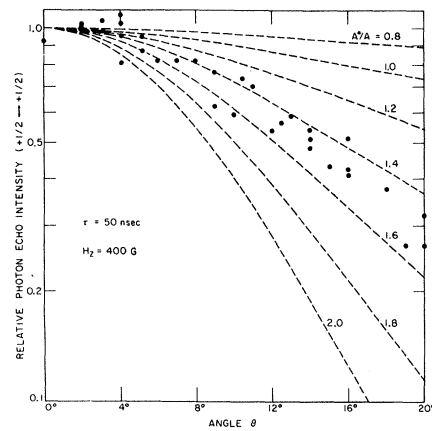

FIG. 11. Comparison of theory for the $(+\frac{1}{2} \longleftrightarrow +\frac{1}{2})$ transition and experiment for the intensity of the photon echoes in ruby with a pulse separation of 50 nsec versus the angle between the optic axis and the applied magnetic field. Data of Abella, Kurnit, and Hartmann (Ref. 10).
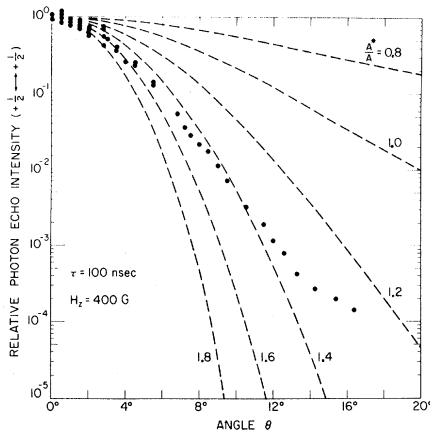
FIG. 12. Comparison of theory for the $(+\frac{1}{2} \longleftrightarrow +\frac{1}{2})$ transition and experiment for the intensity of the photon echoes in ruby with a pulse separation of 100 nsec versus the angle between the optic axis and the applied magnetic field. Data of Abella, Kurnit, and Hartmann, (Ref. 10).

able agreement with experiment. Changing τ from 50 to 100 nsec causes a dramatic change in the Θ dependence, but $A^*/A = 1.4$ gives acceptable agreement with experiment in both cases. Thus, the Θ dependence of the photon echoes seems to be caused by the interactions between the Cr^{3+} ion and the Al nuclear neighbors and to be understandable within the framework of the general theory. Using $A^*/A = 1.4$, which best fits the angular data, we refer to Figs. 13 and 14 (the remaining curves in this section, including Figs. 13 and 14, have been normalized to unity for $\Theta = 0$) and predict that the $\vec{H}$ dependence for $\Theta = 0$ should be negligible when τ is less than 100 nsec and should be observable when τ is of the order of 200 nsec. At first sight these predictions seem to be at variance with the data.[11] However, if one remembers that the above theory is a high-field theory which neglects low-field processes such as mutual spin flips between the Cr^{3+} ion and the Al neighbors, the agreement can be considered acceptable; the observed sharp $\vec{H}$ dependence is due to the low-field processes. Another feature of the data for the field dependence is the sharp dips at 2 and 4 kG, which correspond to the energy level crossings in the $^4A_2$ ground state of the Cr^{3+} ion. For $\Theta \neq 0$, theory predicts a marked reduction in echo intensity for the σ^+ transition at the 2-kG energy-level crossing and for the σ^- transition at the 4-kG crossing, but for $\Theta = 0$, these theoretical dips do not appear. Because the observed echoes were due to echoes from both transitions, two dips would be expected. Figure 14 shows that increasing $\vec{H}$ does not, in general, lead to more intense echoes, and actual reductions in intensity can occur depending on the values of the
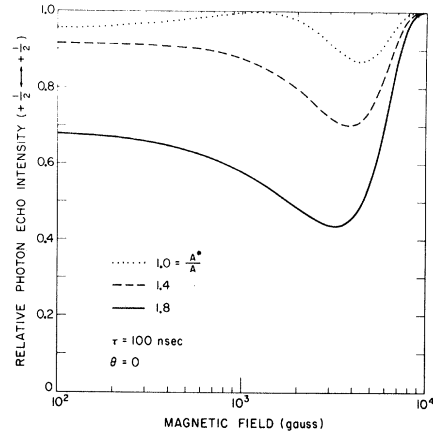

FIG. 13. Theoretical dependence of the intensity of the photon echoes in ruby of the $(+\frac{1}{2} \longleftrightarrow +\frac{1}{2})$ transition with a pulse separation of 100 nsec on the strength of the magnetic field applied along the optic axis.

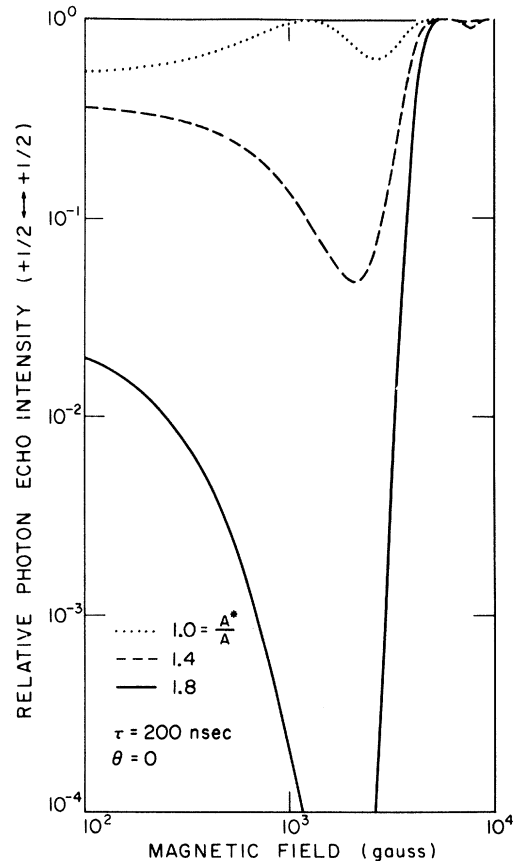interaction constants between the Cr^{3+} ion and the nuclear neighbors. However, in the limit of ex-

FIG. 14. Theoretical dependence of the intensity of the photon echoes of the $(+\frac{1}{2} \longleftrightarrow +\frac{1}{2})$ transition with a pulse separation of 200 nsec on the strength of the magnetic field applied along the optic axis.
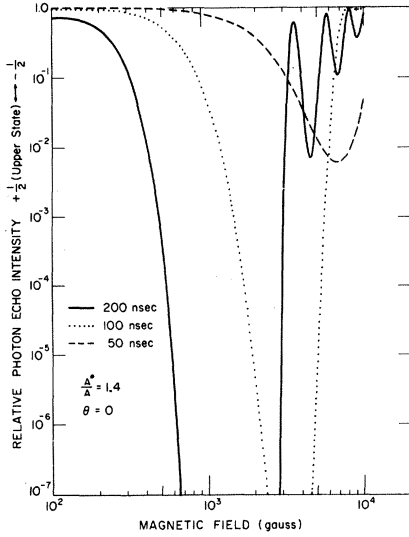
FIG. 15. Theoretical dependence of the intensity of the photon echoes in ruby of the $(+\frac{1}{2}$ upper state $\longleftrightarrow -\frac{1}{2})$ transition on the strength of the magnetic field applied along the optic axis.

tremely high fields, higher than 10 kG, the influence of the nuclei becomes negligible.

Photon echoes associated with the $(+\frac{1}{2}$ upper state $\longleftrightarrow -\frac{1}{2})$ and $(-\frac{1}{2}$ upper state $\longleftrightarrow +\frac{1}{2})$ π transitions have been seen for short pulse separations,[11] but no detailed data are yet available. The theoretical results are much more striking for the π echoes. The predicted $\vec{H}$ and τ dependence for the $(+\frac{1}{2}$ upper state $\longleftrightarrow -\frac{1}{2})$ echoes are shown in Fig. 15 when $\Theta = 0$, and the marked, orders-of-magnitude, $\vec{H}$ dependence with τ of the order of 100 nsec should be easily observable. Figure 16 shows the predicted dynamic τ dependence of these echoes with $\Theta = 0$ and $\vec{H} = 3$ kG.

Photon echoes due to both σ^+ and σ^- transitions have been observed as a function of τ with $\vec{H} \approx 3$ kG nearly parallel to the optic axis; the echo intensity was modulated as τ was varied, and the modulation dramatically increased as Θ was increased.[18] As shown in Fig. 17 for the σ^- transition with $\Theta = 0$ and $\vec{H} = 3$ kG, theory predicts substantial modulation with $A^*/A = 1.4$, and Fig. 18 shows that, if Θ is increased to only $1°$, the photon echo is essentially unobservable for τ between 200 and 300 nsec. However, for the σ^+ transition, the theoretical behavior is quite different. Using the value of $A^*/A = 0.8$ for this transition which best fits the angular fall-off data of Figs. 11 and 12, we obtain Fig. 19 for the Θ and τ dependence of the σ^+ photon echoes. Clearly, more experimental work using circularly polarized excitation pulses is needed, and such photon-echo experiments are in progress to test the main features of the theory and to gain infor-
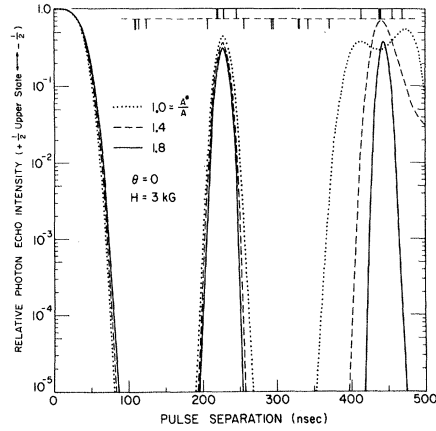

FIG. 16. Theoretical dependence of the intensity of the photon echoes in ruby for the $(+\frac{1}{2}$ upper state $\longleftrightarrow -\frac{1}{2})$ transition on the separation τ between the two excitation pulses with different values of the interaction parameter A^*/A. The short vertical lines below the dashed horizontal line (relative minima for the simple model) mark the values of τ equal to an integral multiple plus one-half of the Larmor periods of the nuclear neighbors with $Q^j = 0$ and $A^*/A = 1.4$; the vertical lines above the dashed line (relative maxima for the simple model) mark the values of τ equal to integral multiples of the Larmor periods.

mation about the interaction constants A^*_j and B^*_j.

V. SIMPLE MODEL
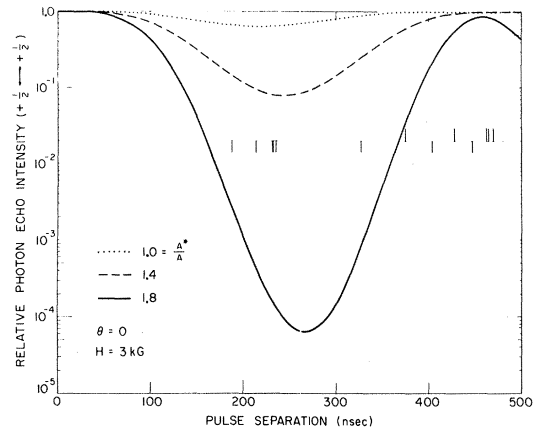
Electron-spin and photon echoes are generally

FIG. 17. Theoretical dependence of the intensity of the photon echoes in ruby for the $(+\frac{1}{2} \longleftrightarrow +\frac{1}{2})$ transition on the separation τ between the two excitation pulses with different values of the interaction parameter A^*/A. The short vertical lines below the horizontal line (relative minima for the simple model) mark the values of τ equal to an integral multiple plus one-half of the Larmor periods of the nuclear neighbors with $Q^j = 0$ and $A^*/A = 1.8$; the vertical lines above the line (relative maxima for the simple model) mark the values of τ equal to integral multiples of the Larmor periods.
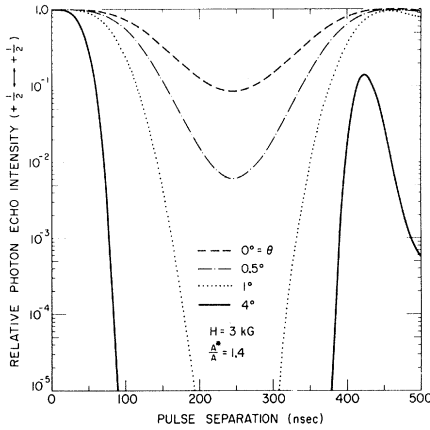
FIG. 18. Theoretical dependence of the intensity of the photon echoes for the $(+\frac{1}{2} \longleftrightarrow +\frac{1}{2})$ transition on the separation between the two excitation pulses and on the angle θ between the magnetic field of 3 kG and the optic axis.

produced by the successive excitation of an ensemble of echo atoms by two intense resonant excitation pulses. In the simplest case, the first pulse induces a precessing macroscopic dipole moment which soon decays because the dipole moments of the individual echo atoms precess at slightly different frequencies because of their different local environments. It is well known[19,20] that the second pulse (considered to be a 180° pulse) negates the relative phase of these precessing dipoles. If the local environment of each echo atom is constant, the dipoles, after the second pulse, will rephase at the same rate at which they had dephased, and the macroscopic moment will reform to produce the echo. To the extent that the local environments fluctuate in time, the rephasing is incomplete, and as the pulse separation is increased an exponential decay of the echo amplitude is usually observed. The surprising behavior of the spin and photon echoes from isolated echo atoms in ionic crystals is that in many cases the echo amplitude oscillates between quite large and small values as the pulse separation is increased. This echo modulation is caused by the slow (compared to the precession frequency of the dipoles) regular time dependence of the local environments of the echo atoms, which is due to the precession of the magnetic nuclei of the neighboring atoms.

The excitation pulses are assumed to couple together only the two echo states of the echo atom, and for an understanding of the echo behavior, the echo atom can be considered as a simple two-level system. The echo states are designated as states 1 and 2, where state 1 has the higher energy. The time dependence of the local environment due to the precession of the nuclear neighbors of the echo

atom causes the energy separation $\omega(t)$ between the two echo states to be time dependent. $\omega(t)$ can be separated into the two terms

$$\omega(t) = \omega_0 + \delta(t) \quad . \tag{5.1}$$

$\delta(t)$ describes the effect of the neighbors on the echo atom and has a time-dependent part which is responsible for the dephasing; ω_0 is the constant energy separation between the two echo states in the absence of the neighboring nuclei. $\delta(t)$ is usually very small compared to ω_0; for photon echoes $\delta(t) \approx 10^{-8} \omega_0$ and for electron-spin echoes $\delta(t) \approx 10^{-4} \omega_0$.

Consider the echo atom to interact with only one nuclear neighbor which has no electric quadrupole moment, and let the Hamiltonain for the echo atom and the neighbor be given by

$$\mathcal{H} = \frac{1}{2}\hbar\omega_0\sigma_3 + A\vec{S}\cdot\vec{I}$$
$$+ B\vec{S}\cdot[3\vec{r}(\vec{r}\cdot\vec{I})/r^5 - \vec{I}/r^3] - \hbar\gamma\vec{H}\cdot\vec{I} \quad . \tag{5.2}$$

$\vec{S}$ and $\vec{I}$ are the spin operators for the echo atom and the neighbor, respectively. $\vec{H}$ is the applied magnetic field, and $\vec{r}$ is the vector from the atom to the neighbor. Equation (5.2) can be rewritten in the simpler form

$$\mathcal{H} = \frac{1}{2}\hbar\omega_0\sigma_3 - \hbar\gamma\vec{H}_\epsilon\cdot\vec{I} \quad , \tag{5.3}$$

where $\vec{H}_\epsilon$ is an operator that describes an effective magnetic field[8] at the neighbor site. Define the two quantities

$$\vec{H}_\epsilon^1 \equiv \langle 1|\vec{H}_\epsilon|1\rangle \quad \text{and} \quad \vec{H}_\epsilon^2 \equiv \langle 2|\vec{H}_\epsilon|2\rangle \quad . \tag{5.4}$$

$|1\rangle$ and $|2\rangle$ are the eigenfunctions for the echo states 1 and 2. $\vec{H}_\epsilon^1$ or $\vec{H}_\epsilon^2$ is the effective field for the nuclear neighbor when the echo atom is in state 1 or 2, respectively.
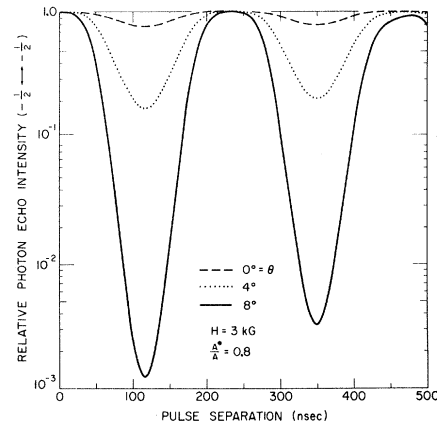

FIG. 19. Theoretical dependence of the intensity of the photon echoes for the $(-\frac{1}{2} \longleftrightarrow -\frac{1}{2})$ transition on the separation between the two excitation pulses and on the angle θ between the magnetic field of 3 kG and the optic axis.

tively. Because the second term in Eq. (5.3) is very small compared to the first, the expression for $\omega(t)$ can be immediately written

$$\hbar\omega(t) = \langle 1|\mathcal{3C}|1\rangle - \langle 2|\mathcal{3C}|2\rangle \quad , \qquad (5.5)$$

which is equivalent to

$$\omega(t) = \omega_0 - \gamma[\vec{H}_\epsilon^1 - \vec{H}_\epsilon^2]\cdot\vec{I}(t) \quad . \qquad (5.6)$$

The simple model treats the nuclear spin vector $\vec{I}(t)$ as a classical quantity. Thus, once the motion of $\vec{I}(t)$ is known, Eq. (5.6) allows the echo behavior due to the interaction between the echo atom and the nuclear neighbor to be calculated. If the echo atom were in either echo state 1 or 2, the motion of $\vec{I}(t)$ would be a precession about $\vec{H}_\epsilon^1$ or $\vec{H}_\epsilon^2$. When the echo atom is in a linear superposition of states (partially in state 1 and partially in state 2), calculation of the expectation value of $\vec{I}$ gives a result that corresponds to the vector summation of two precessing vectors, where one vector precesses about $\vec{H}_\epsilon^1$ with angular frequency ω_1 and the other precesses about $\vec{H}_\epsilon^2$ with angular frequency ω_2. Thus, when the echo atom is in a linear superposition of states we write

$$\vec{I}(t) = \vec{I}_1(t) + \vec{I}_2(t) \quad , \qquad (5.7)$$

where we interpret $\vec{I}_1(t)$ as precessing about $\vec{H}_\epsilon^1$ with angular frequency ω_1 and $\vec{I}_2(t)$ as precessing about $\vec{H}_\epsilon^2$ with frequency ω_2:

$$\omega_1 = \gamma|\vec{H}_\epsilon^1| \quad\text{and}\quad \omega_2 = \gamma|\vec{H}_\epsilon^2| \quad . \qquad (5.8)$$

If the echo atom is equally in states 1 and 2, the magnitudes of $\vec{I}_1(t)$ and $\vec{I}_2(t)$ are the same. This description is certainly correct when the echo atom is completely in state 1 or 2 and is the simplest behavior we can ascribe to the nuclear spin vector to explain the observed modulated echo behavior in an intuitive way. Referring to Eqs. (5.1) and (5.6), we see that in terms of the simple model, the time dependence of $\delta(t)$ is given by two sinusoidal components, one oscillating at ω_1 and the other at ω_2. As the time-dependent parts of $\vec{I}_1(t)$ and $\vec{I}_2(t)$ are orthogonal to $\vec{H}_\epsilon^1$ and $\vec{H}_\epsilon^2$, respectively, only the projections of the time-dependent parts of $\vec{I}_1(t)$ on $\vec{H}_\epsilon^2$ and $\vec{I}_2(t)$ on $\vec{H}_\epsilon^1$ are nonzero, and consequently, evaluation of Eq. (5.6) shows that the amplitudes of the two sinusoidal components of $\delta(t)$ are proportional to the sine of the angle Δ between $\vec{H}_\epsilon^1$ and $\vec{H}_\epsilon^2$. These results are easily extended to an echo atom with more than one nuclear neighbor. For this situation, $\delta(t)$ is again given by a sum of sinusoidal components with two components for each neighbor, and the amplitudes of the components for the jth neighbor are proportional to the sine of the angle Δ_j between the two effective fields for the jth neighbor.

The fact that $\delta(t)$ is given by a sum of sinusoidally oscillating components allows for the partial re-phasing that is necessary to obtain the spin or photon echoes. The most general condition for the occurrence of the two-pulse echo is that the integrals of $\delta(t)$ with respect to time after each of the two excitation pulses be the same for all the echo atoms. This requirement will be satisfied for a single oscillating component of $\delta(t)$, independent of the phase of the oscillation (the phase varies randomly from echo atom to echo atom) when the separation between the two pulses is equal to an integral multiple of the period of the oscillation. Usually $\delta(t)$ is composed of many components, and the rephasing condition cannot be satisfied for all of them simultaneously. Thus, only relative maxima in the echo signal are expected when the pulse separation is equal to integral multiples of the periods of the oscillating components. If the magnitude of $\delta(t)$ is increased, the dephasing effects of the components for which the rephasing condition is not satisfied will become much larger and the echo signals will be rapidly reduced.

The simple model can be applied to both electron-spin and photon echoes in ruby, since the echo dephasing caused by the nuclear neighbors is independent of the energy separation ω_0 between the two echo states if ω_0 is large compared to the interaction energy between Cr^{3+} ion and the nuclear neighbors. However, the spin-echo signals are proportional to the macroscopic dipole moment of the system at $t = 2\tau$, and the photon echoes are proportional to the square of the macroscopic moment at $t = 2\tau$. Thus, an equivalent amount of dephasing would appear much more intense for photon echoes than for spin echoes. The Cr^{3+} ion which is responsible for the echo radiation in both cases interacts quite strongly with the magnetic nuclei of the 13 nearest Al neighbors.[8] If the angle Θ between the applied magnetic field $\vec{H}$ and the optic axis is zero, the angle Δ between the two effective fields for the nearest neighbor is zero, and this neighbor does not contribute to the echo dephasing. The remaining 12 neighbors form four groups each composed of three equivalent neighbors; all the members of a group dephase the echo in the same way. The strengths of the components for a group are proportional to $\sin\Delta$ for the equivalent nuclei of the group.

Because the Al nuclei have an electric-quadrupole moment, $\delta(t)$ contains so many components that application of the model for obtaining the echo envelope is difficult when the pulse separations are large compared to the period of the quadrupolar splitting (the spin-echo case). However, for photon echoes excited by pulses less than 0.5 μsec apart the problem could be simplified by neglecting the quadrupole splitting. For $\Theta = 0$ $\delta(t)$ can then be resolved into eight sinusoidal components, where

each group contributes two components, and in Figs. 16 and 17 the relative maxima and minima are easily observed.

When $\vec{H}$ is tilted away from the optic axis, the 13 neighbors become inequivalent, but for relatively small values of Θ the most important change is that as Θ is increased $\delta(t)$ sharply increases. $\delta(t)$ has a relative minimum for $\vec{H}$ parallel to the optic axis, because the Δ_j angles of the individual neighbors are smallest when $\Theta = 0$. As was noted earlier,[4] in many cases the Δ_j angles increase much faster than Θ, as Θ is increased. This feature explains the angular dependence of both spin and photon echoes. As Θ is increased, $\delta(t)$ increases, and the echo signals are reduced. The reduction occurs regardless of the pulse separation, because the rephasing condition cannot be satisfied simultaneously for all the components. The dips observed in the photon-echo signals for $\vec{H} = 2$ and 4 kG with $\Theta = 0$ occur at the energy-level crossings in the $^4A_2$ ground state of the Cr^{3+} ion. At these crossings $\delta(t)$ is a very sharp function of Θ, and a small increase in Θ leads to a large reduction in the echo signal. As the optic axis varies by about 1 degree throughout the crystal, reductions in the echo signals are expected at the crossings. In the theoretical results for the spin echoes, the very large difference between the predicted echo amplitudes of the $(+\frac{1}{2} \longleftrightarrow +\frac{3}{2}$ low field) and the $(+\frac{1}{2} \longleftrightarrow +\frac{3}{2}$ high field) transitions is due to the difference between the Δ_j angles for the two field values. The Δ_j angles are much smaller for the high-field transition than for the low-field transition. Similarly, for the photon echoes the marked difference between the theoretical behavior of the echoes of the $(+\frac{1}{2} \longleftrightarrow +\frac{1}{2})$ transition and the $(+\frac{1}{2} \longleftrightarrow -\frac{1}{2})$ transition is mainly due to the Δ_j angles being much smaller for the $(+\frac{1}{2} \longleftrightarrow +\frac{1}{2})$ transition than for the $(+\frac{1}{2} \longleftrightarrow -\frac{1}{2})$ transition.

ACKNOWLEDGMENTS

[1]W. B. Mims, K. Nassau, and J. D. McGee, Phys. Rev. 123, 2059 (1961).

[2]J. A. Cowen and D. E. Kaplan, Phys. Rev. 124, 1098 (1961).

[3]L. G. Rowan, E. L. Hahn, and W. B. Mims, Phys. Rev. 137, A61 (1965).

[4]D. Grischkowsky and S. R. Hartmann, Phys. Rev. Letters 20, 41 (1968).

[5]A. K. Saha and T. P. Das, Theory and Applications of Nuclear Induction (Saha Institute of Nuclear Physics, Calcutta, India, 1957).

[6]A. Abragam, The Principles of Nuclear Magnetism (Oxford U. P., London, England, 1969).

[7]G. M. Zhidomirov and K. M. Salikov, Teor. i Eksperim. Khim. 4, 514 (1968).

[8]N. Laurance, E. C. McIrvine, and J. Lambe, J. Phys. Chem. Solids 23, 515 (1962).

[9]N. A. Kurnit, I. D. Abella, and S. R. Hartmann, Phys. Rev. Letters 13, 567 (1964).

[10]I. D. Abella, N. A. Kurnit, and S. R. Hartmann, Phys. Rev. 141, 391 (1966).

[11]N. A. Kurnit and S. R. Hartmann, in Interaction of Radiation with Solids (Plenum, New York, 1967), pp. 693-701.

[12]A. Compaan, L. Q. Lambert, and I. D. Abella, Phys. Rev. Letters 20, 1089 (1968).

[13]For photon echoes, ω_0 is approximately 10^8 times larger than the nuclear frequencies and the neglect of H_{12}^I and H_{21}^I is always correct. For electron-spin echoes, if the strength of $\vec{H}$ is sufficient to put ω_0 in the microwave range, in most cases ω_0 is of the order of 10^4 times larger than the nuclear frequencies, and H_{12}^I and H_{21}^I can be neglected. However, for spin echoes, if $\vec{H}$ is small, ω_0 can be of the order of the nuclear frequencies, and H_{12}^I and H_{21}^I must be retained; in the following work we assume $\vec{H}$ is large enough so that neglect of H_{12}^I and H_{21}^I is valid.

[13a]The arbitrary phase $2\tau\omega_0$ is determined by the assumed form of R_1 and R_2.

[14]E. O. Schultz-DuBois, Bell System Tech. J. 38, 271 (1959).

[15]A. M. Clogston, Phys. Rev. 118, 1229 (1960).

[16]S. Geschwind, G. E. Devlin, R. L. Cohen, and S. R. Chinn, Phys. Rev. 137, A1087 (1965).

[17]S. Geschwind, R. J. Collins, and A. L. Schawlow Phys. Rev. Letters 3, 545 (1959).

[18]I. D. Abella, A. Compaan, and L. Q. Lambert, Bull. Am. Phys. Soc. 14, 115 (1953).

[19]E. L. Hahn, Phys. Today 6, 4 (1953).

[20]H. Y. Carr and E. M. Purcell, Phys. Rev. 94, 630 (1954).